



Original article

RNA sequencing reveals the long noncoding RNA and mRNA profiles and identifies long non-coding RNA TSPAN12 as a potential microvascular invasion-related biomarker in hepatocellular carcinoma

Jiong Lu^{a,1}, Bei Li^{b,1}, Xianze Xiong^a, Nansheng Cheng^{a,*}^a Department of Bile Duct Surgery, West China Hospital, Sichuan University, Chengdu, Sichuan, 610041, China^b West China-Washington Mitochondria and Metabolism Research Center, West China Hospital, Sichuan University, Chengdu, Sichuan, 610041, China

ARTICLE INFO

ABSTRACT

Keywords:
 Hepatocellular carcinoma
lnc-TSPAN12
 Long noncoding RNA
 Microvascular invasion
 RNA-seq

Emerging evidence demonstrates that abnormally expressed long noncoding RNAs (lncRNAs) are involved in the progression of various cancers. However, the expression profiles and functions of lncRNAs in hepatocellular carcinoma (HCC) with microvascular invasion (MVI) remain largely unknown. In this study, we revealed the differential expression profiles of lncRNA and messenger RNA in four pairs of HCC with MVI and adjacent nontumor liver tissues by using high-throughput RNA sequencing. Among these dysregulated lncRNAs, *lnc-TSPAN12* was the most significantly upregulated lncRNA in HCC. The results of real time-PCR showed that *lnc-TSPAN12* was highly expressed in HCC, including HCC with MVI, and its high expression was associated with unfavorable clinicopathological features and poor prognosis. Moreover, multivariate Cox regression analysis verified that *lnc-TSPAN12* was an independent prognostic predictor for overall and recurrence-free survival. Receiver operating characteristic curve analysis indicated that *lnc-TSPAN12* could serve as a potential diagnostic biomarker for HCC with MVI. In addition, a loss-of-function experiment demonstrated that *lnc-TSPAN12* knockdown inhibited HCC cell migration and invasion in vitro. Our findings suggest that *lnc-TSPAN12* may function as an oncogene in HCC progression and could serve as a novel diagnostic/prognostic biomarker and potential therapeutic target for HCC with MVI.

1. Introduction

Hepatocellular carcinoma (HCC), which accounts for over 90 % of primary liver cancers, is one of the most common malignancies and the third leading cause of cancer-related deaths worldwide [1]. Despite considerable advancement in HCC diagnosis and treatment, the long-term survival rate of HCC remains low due to high recurrence and metastasis rates [2,3]. Microvascular invasion (MVI) has been confirmed to be strongly associated with early recurrence and poor survival outcomes in HCC after surgical resection [4–6]. Therefore, novel biomarkers and effective therapeutic targets for HCC with MVI must be identified.

Over the past decade, advances in high-throughput RNA sequencing (RNA-seq) technology and bioinformatic analysis have facilitated the research on the entire human genome sequence, including long non-coding RNAs (lncRNAs). lncRNAs represent a class of transcripts that are greater than 200 nt in length and have no protein-coding potential [7,8]. Accumulated evidence suggests that lncRNAs are important regulators involved in various cellular biological processes [9]. The aberrant expression of lncRNAs plays critical roles in cancer progression [10], including HCC [11–13]. For example, *lncRNA MVIH* (lncRNA associated with MVI in HCC) can promote angiogenesis by inhibiting the secretion of *PGK1* and serve as a predictor for poor recurrence-free survival (RFS) of patients with HCC after liver resection [13]. A recent

Abbreviations: HCC, hepatocellular carcinoma; MVI, microvascular invasion; lncRNA, long noncoding RNA; RNA-seq, RNA sequencing; MVIH, LncRNA associated with microvascular invasion; PGK1, phosphoglycerate kinase1; RFS, recurrence-free survival; PTTG3P, pituitary tumor-transforming 3, pseudogene; PI3K, phosphatidylinositol-3-kinase; AKT, protein kinase B; mRNA, messenger RNA; ANLT, adjacent nontumor liver tissue; GO, gene ontology; KEGG, Kyoto encyclopedia of genes and genomes; qRT-PCR, quantitative real-time polymerase chain reaction; CCK-8, cell counting kit 8; SD, standard deviation; OS, overall survival; ROC, receiver operating characteristic; AFP, alpha-fetoprotein

* Corresponding author at: Department of Bile Duct Surgery, West China Hospital, Sichuan University, 37# Guoxue Road, Chengdu, 610041, Sichuan Province, China.

E-mail address: nanshengcheng@163.com (N. Cheng).

¹ These authors are co-first authors.

<https://doi.org/10.1016/j.biopha.2020.110111>

Received 5 January 2020; Received in revised form 14 March 2020; Accepted 17 March 2020

0753-3322/© 2020 The Authors. Published by Elsevier Masson SAS. This is an open access article under the CC BY-NC-ND license (<http://creativecommons.org/licenses/by-nd/4.0/>).

study confirmed that *lncRNA PTTG3P* promotes tumor growth and metastasis by upregulating *PTTG1* and activating *PI3K/AKT* signaling in HCC [14]. These results indicate that lncRNAs might serve as novel biomarkers and potential therapeutic targets for HCC. However, given that most lncRNAs remain largely unknown, further study is needed to elucidate their function and molecular mechanism.

In the present study, we revealed the differential expression profiles of lncRNA and messenger RNA (mRNA) in four pairs of HCC with MVI and adjacent nontumor liver tissues (ANLTs) by using high-throughput RNA-seq. Among the dysregulated lncRNAs, we demonstrated that *lnc-TSPAN12* might play an oncogenic role in HCC progression and act as a potential diagnostic and prognostic biomarker for HCC with MVI.

2. Material and methods

2.1. Clinical specimens and cell lines

A total of 62 pairs of HCC tissues and their corresponding ANLT were obtained from West China Hospital of Sichuan University between January 2013 and December 2015. Another 80 pairs of HCC with MVI and their corresponding ANLTs were collected from the same hospital between March 2017 and June 2019. The specimens were immediately frozen in liquid nitrogen after resection and stored at -80°C until RNA extraction. None of the patients received any preoperative chemotherapy, radiotherapy, or targeted therapy. Informed consent was obtained from each patient, and the protocols of this study were approved by the Ethics Committee of West China Hospital Permit No. 20190304 dated March 4, 2019. The demographic and clinicopathologic features of the 62 patients with HCC are described in Table 1. Human HCC (i.e., HepG2, Huh-7, Bel-7402, and MHCC97-H) and the human normal hepatocyte cell line (i.e., LO2) were purchased from the Institute of Biochemistry and Cell Biology (Chinese Academy

Table 1
Correlations between *lnc-TSPAN12* and clinicopathologic features in HCC.

Clinicopathological parameters	Total (n = 62)	<i>lnc-TSPAN12</i> expression ^a		<i>P</i>
		Low(n = 31)	High(n = 31)	
Age (years)				
< 50	36	17	19	0.607
≥ 50	26	14	12	
Gender				
Male	47	24	23	0.767
Female	15	7	8	
AFP (ng/ml)				
< 20	18	11	7	0.263
≥ 20	44	20	24	
Tumor size (cm)				
≤ 5	20	14	6	0.030
> 5	42	17	25	
Tumor number				
Single	45	22	23	0.776
Multiple	17	9	8	
Capsule formation				
No	37	18	19	0.796
Yes	25	13	12	
Macrovascular invasion				
No	38	23	15	0.037
Yes	24	8	16	
Microvascular invasion				
No	29	19	10	0.022
Yes	33	12	21	
TNM staging				
I/II	26	17	9	0.039
III/IV	36	14	22	
Edmondson-Steiner grade				
I-II	30	17	13	0.309
III-V	32	14	18	

HCC, hepatocellular carcinoma; AFP, alpha-fetoprotein.

^a Using median expression level of *lnc-TSPAN12* as cutoff.

of Sciences, Shanghai, China). All cells were cultured in complete DMEM (Thermo Fisher Scientific, Waltham, MA, USA) supplemented with 10 % fetal bovine serum (FBS; HyClone, USA) and incubated at 37°C in a humidified incubator with 5% CO₂.

2.2. High-throughput RNA-seq analysis

High-throughput RNA-seq analysis was conducted by OE Biotechnology Co., Ltd (Shanghai, China). In brief, total RNAs were isolated separately from four pairs of HCC tissues and their corresponding ANLT by using the TRIzol reagent (Invitrogen, Carlsbad, CA, USA). Then, the RNA quality and concentration were evaluated using an Agilent 2100 Bioanalyzer (Agilent Technologies, Santa Clara, CA, USA) and a ND1000 spectrophotometer (NanoDrop, Wilmington, DE, USA), respectively. A total of 5 μg RNA per sample was used for the preparations. After ribosomal RNA (rRNA) was digested by TruSeq Stranded Total RNA with Ribo-Zero Gold Kit (Illumina, Inc., San Diego, CA, USA), the rRNA-removed RNA was fragmented into short pieces, and the cDNA library was constructed using the NEBNext Ultra RNA Library Prep Kit for Illumina (NEB, Ipswich, MA, USA). The libraries were sequenced on an Illumina HiSeq 3000 platform (Illumina Inc., San Diego, CA, USA) in accordance with the manufacturer's instructions.

2.3. Bioinformatic analysis

The sequencing quality of the raw data of the FASTQ format was assessed with FastQC software [15]. Low-quality data were filtered with Trimmomatic software [16]. To obtain location information on the reference genome or gene and the unique sequence information of the sequencing samples, we aligned the high-quality clean reads to the human reference genome by using HISAT2 [17]. FDR or the *q* value was corrected for multiple hypothesis testing. DESeq2 software was used to calculate the fold change and significant difference. *P*-value < 0.05 and fold change > 1 were used as the threshold to screen significant differentially expressed genes.

2.4. Function enrichment analysis

We performed gene ontology (GO) enrichment and Kyoto Encyclopedia of Genes and Genomes (KEGG) pathway analyses on the differentially expressed mRNAs and *lnc-TSPAN12* by using KOBAS 3.0 software. The GO terms and KEGG pathways with corrected *P*-value < 0.05 were significantly enriched.

2.5. LncRNA–mRNA co-expression network

The lncRNA–mRNA co-expression network was established using Cytoscape software to investigate the relationship between differentially expressed lncRNAs and mRNAs. The Pearson correlation coefficients between differentially expressed lncRNAs and mRNAs were calculated and compared with the *R* value. A Pearson's correlation coefficient ≥ 0.80 and a *P*-value < 0.05 were considered statistically significant.

2.6. RNA extraction and quantitative real-time polymerase chain reaction analysis

The total RNA from HCC tissues and cells was isolated using the TRIzol reagent (Invitrogen, Carlsbad, CA, USA) according to the manufacturer's protocol. cDNA synthesis was performed with 2 mg of total RNA by using a reverse transcription kit (Takara Bio, Kusatsu, Japan). Quantitative real-time PCR (qRT-PCR) was performed with the SYBR Green Master Mixture. The relative lncRNA expression level was normalized to the GAPDH expression. The primers used in qRT-PCR were designed with RocheLCPDS2 software and ordered from Genecopoeia (Guangzhou, China) (Table S1, Supplementary Materials). The relative

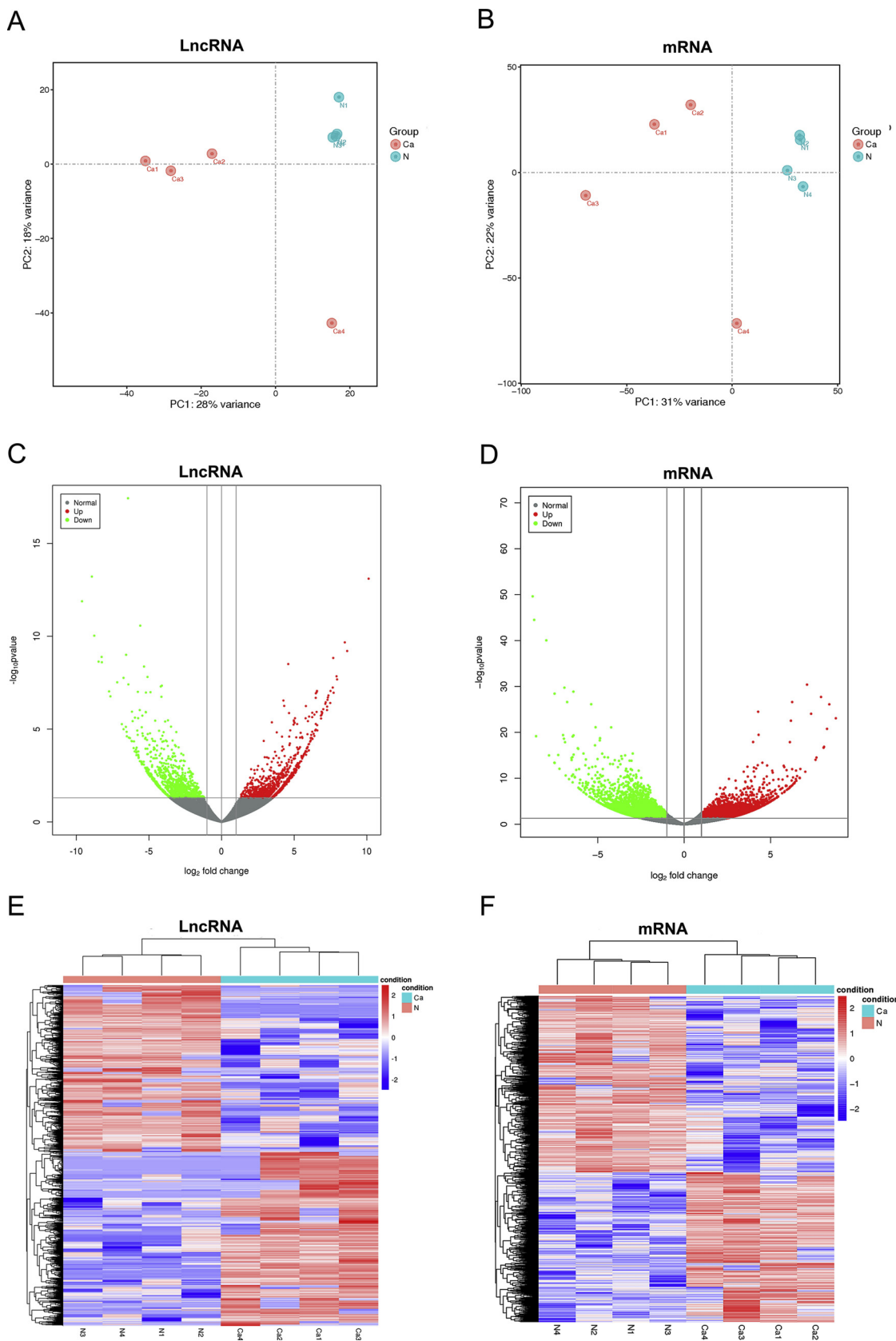


Fig. 1. RNA-seq reveals distinct expression profiles of lncRNA and mRNA in HCC with MVI and ANLT. (A-B) PCA plot of lncRNAs and mRNAs expression profiles. (C-D) Volcano plot displayed the differentially expressed lncRNAs and mRNAs between HCC with MVI and ANLT. X-axis: the fold change expressed as log2; Y-axis: expressed by P value. The horizontal gray lines represented a P value of 0.05, and the vertical gray lines corresponded to two-fold up- and down-regulation. (E-F) Hierarchical clustering heatmap of the dysregulated lncRNAs and mRNAs between HCC with MVI and ANLT. The expression values were represented by a color scale. Ca, HCC tissues; N, adjacent nontumor liver tissues.

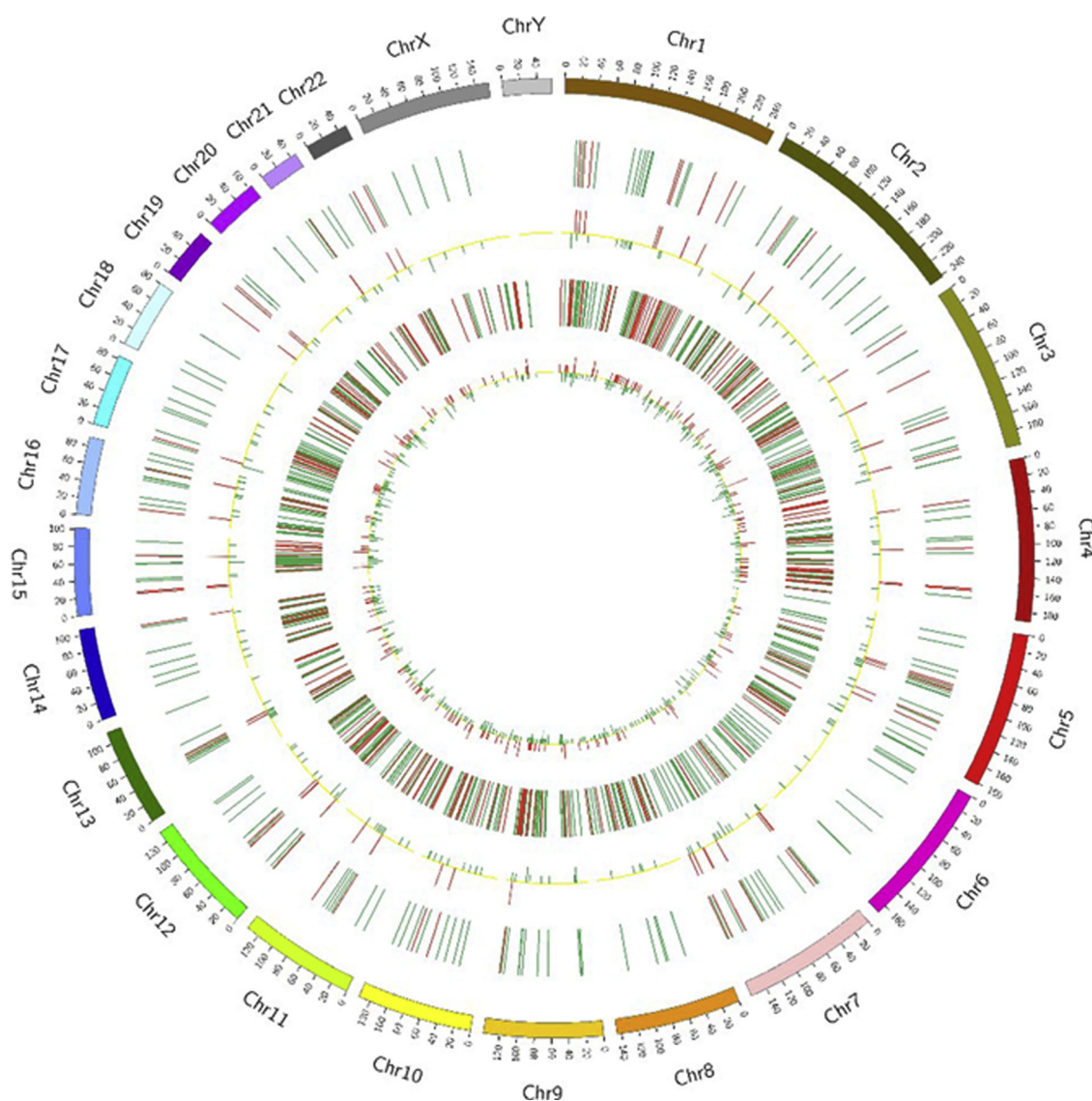


Fig. 2. Circos plots shows the distribution of differentially expressed lncRNAs and mRNAs on human chromosomes. The outermost layer cycle was the chromosome map of the human genome. The inner layers from outside to inside represented the distribution of differentially expressed lncRNAs and mRNA on different chromosomes, respectively. Red and green colors indicated up- and down-regulation, respectively.

expression of lncRNAs was calculated with the $2^{-\Delta\Delta Ct}$ method normalized to endogenous control.

2.7. Vector constructs and transfection

The validated shRNA sequence of lnc-TPSAN12 was synthesized by Shanghai R&S Biotechnology Co. (Shanghai, China) and cloned into the eukaryotic expression vector pcDNA6.2-EGFP-miR and the lentiviral expression vector plenti6.3-mcs. The siRNAs of lnc-TPSAN12 were purchased from Sangon Biotech (Shanghai, China).

The transfection of plasmids or siRNAs was performed with the Polo Deliverer 3000 transfection reagent according to the manufacturer's instructions. Transduction with lentivirus was performed using 2 mg/ml polybrene (Sigma-Aldrich), and positive cells were selected with puromycin (Sigma-Aldrich). The efficiency of lnc-TPSAN12 knockdown was detected through qRT-PCR.

2.8. Cell proliferation, migration, and invasion assays

A cell proliferation assay was performed with cell counting kit 8 (CCK-8) (Dojindo Laboratories, Kumamoto, Japan) following the

manufacturer's instructions. Huh 7 cells were seeded onto 96-well plates at a concentration of 4000 cells/well. After 24 h, the cells in each well were added with 10 μ l of CCK-8 and incubated at 37 °C for 2 h. Subsequently, the optical density at a wavelength of 450 nm was read using a microplate reader Thermo Fisher Scientific, Waltham, MA, USA. Cell migration and invasion assays were also performed using 24-well Transwell chambers Corning, NY, USA with or without Matrigel coating BD Biosciences, Franklin Lakes, NJ, USA. In brief, 1×10^5 transfected cells were suspended in serum-free DMEM medium in the upper chamber, and DMEM medium containing 20 % FBS was added to the lower chamber. After 24 h, migrating/invasive cells were fixed with methanol and stained with 0.1 % crystal violet. Photographs of five randomly selected views of the fixed cells were obtained, and cell numbers were calculated under a microscope. All experiments were performed three times.

2.9. Statistical analysis

All data are presented as means \pm standard deviation (SD). Statistical analyses were conducted using GraphPad Prism 7.0 (GraphPad Software, Inc. La Jolla, CA, USA) and SPSS software (v.21.0;

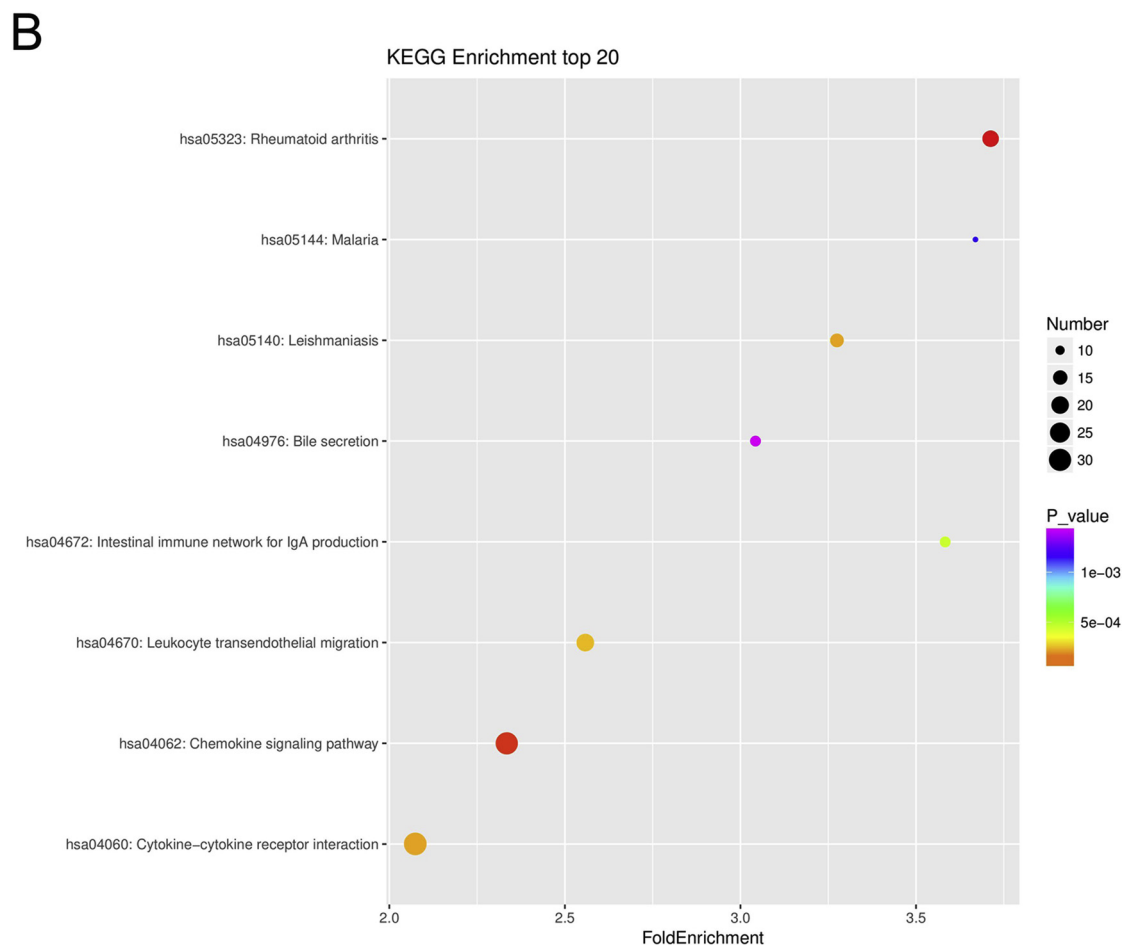
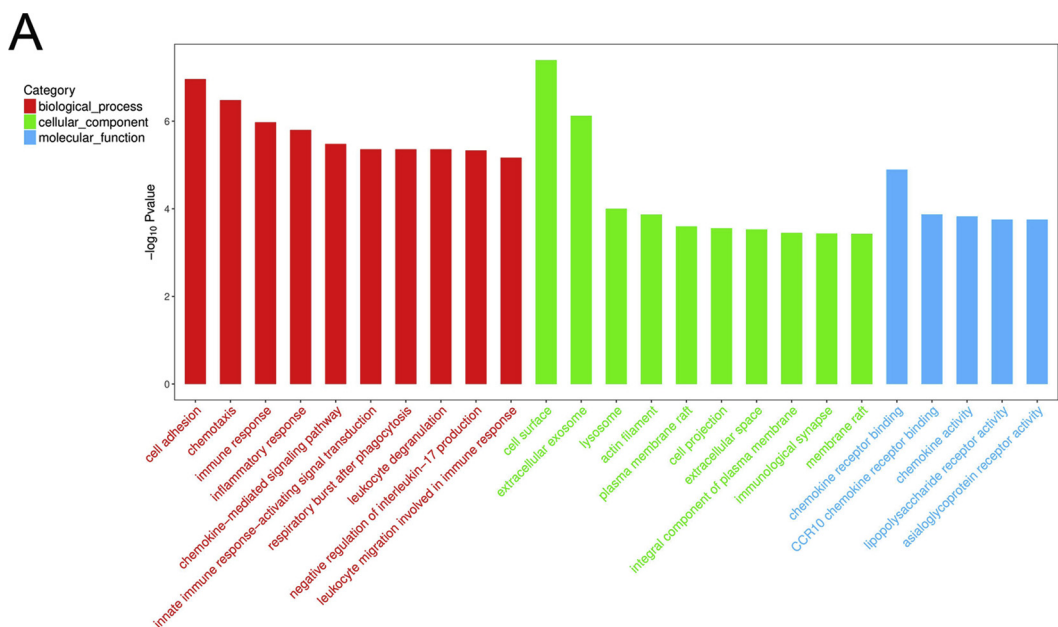


Fig. 3. GO and KEGG analyses of the differentially expressed mRNAs. (A) GO annotation of the differentially expressed mRNAs. The bar plot presented the enrichment scores ($-\log_{10}$ [p value]) of top 10 significantly enriched GO terms in biological processes, cellular components and molecular functions. (B) Bulb map of KEGG analysis for the differentially expressed mRNAs. X-axis indicated the enrichment score of differentially expressed genes. Y axis revealed the name of enriched pathways. The size of node represented the number of enriched differential genes. The P-value was represented by a color scale, which suggested that the statistical significance increased as purple turn to red.

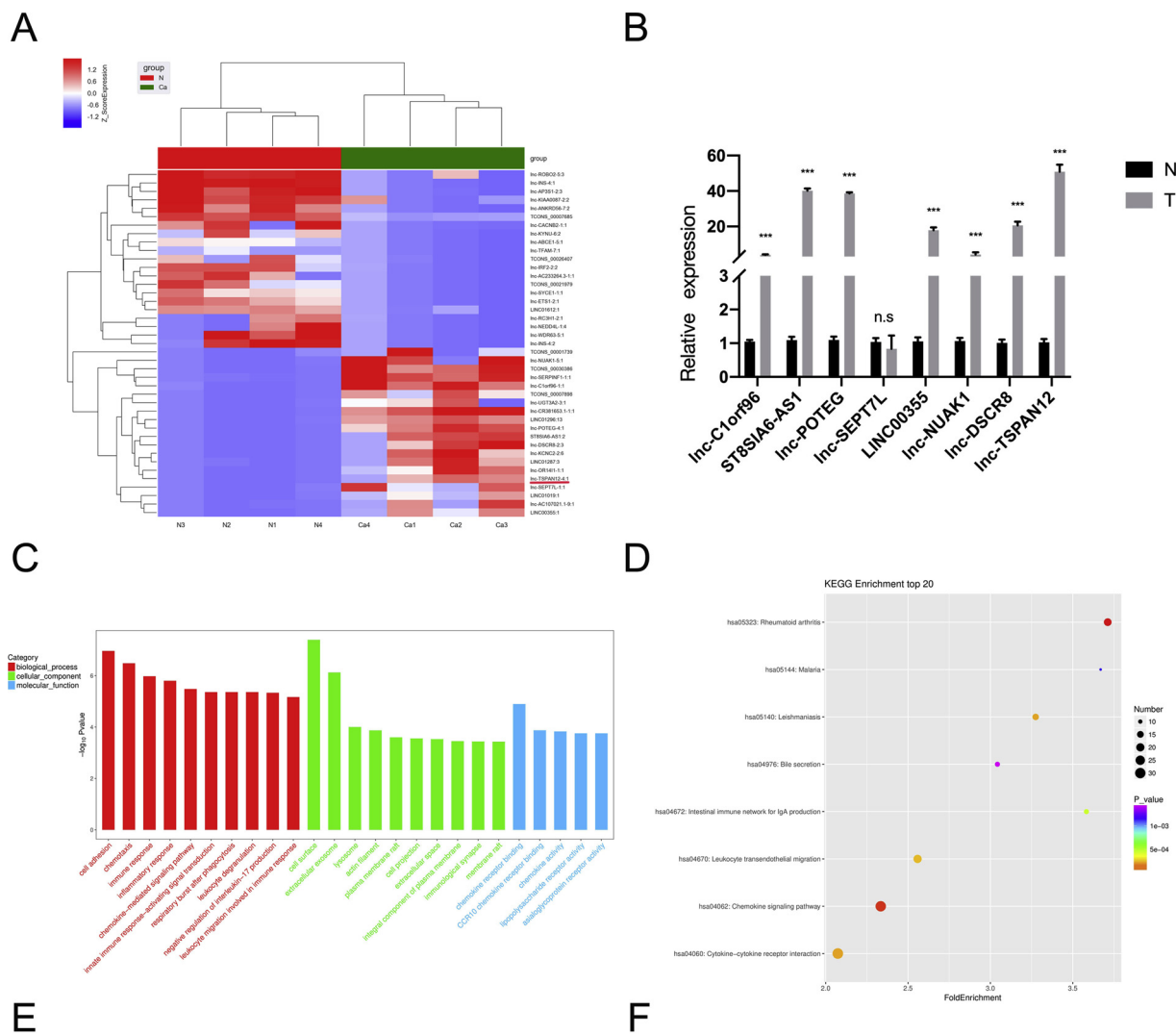


Fig. 4. QRT-PCR validation and bioinformatic analyses identify *lnc-TSPAN12* as a candidate lncRNA for further investigation. (A) Hierarchical clustering heatmap of the top 20 dysregulated lncRNAs between HCC with MVI and ANLT. (B) qRT-PCR validation of eight up-regulated lncRNAs expression (randomly selected from the top 20 up-regulated lncRNAs) in 10 pairs of HCC with MVI and ANLT. (C-D) GO and KEGG analyses of *lnc-TSPAN12*. E, Genome browser showed the genomic location and sequence full-length of *lnc-TSPAN12*. F, CPAT website predicted the ability to encode proteins of *lnc-TSPAN12*. * $P < 0.05$, ** $P < 0.01$, *** $P < 0.001$. T, HCC tissues; N, adjacent nontumor liver tissues.

IBM, Armonk, NY, USA). The statistical differences between the two groups were determined through an independent Student's *t*-test. The χ^2 test or Fisher's exact test was used to analyze the relationship between *lnc-TSPAN12* expression and clinicopathologic characteristics. The Kaplan-Meier method was adopted to evaluate the differences in the overall survival (OS) and RFS. Univariate and multivariate Cox regression analyses were performed to determine the independent prognostic factors for OS and RFS. Co-expression networks were drawn using Cytoscape software 3.2.0. Differences with $P < 0.05$ were considered statistically significant.

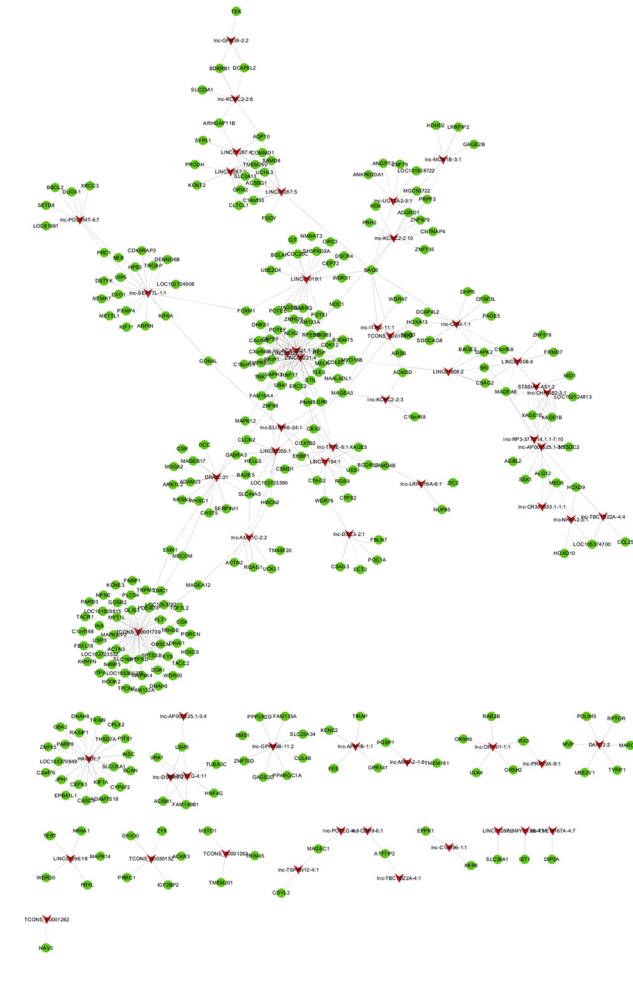
3. Results

3.1. Profiles of differentially expressed lncRNA and mRNA in HCC

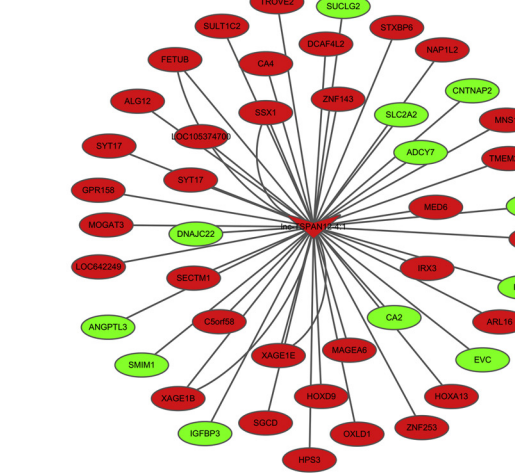
We analyzed lncRNA and mRNA expression profiles in the four pairs of HCC with MVI and ANLT by using high-throughput RNA-seq

analysis. The characteristic details of the four samples are listed in Supplementary Table S2. A total of 4005 and 98,122 lncRNA and mRNA transcripts were detected by RNA-seq, respectively. Out of the lncRNA and mRNA transcripts, 933 novel lncRNAs were identified, including 461 intergenic lncRNAs, 180 antisense lncRNAs, 45 intronic lncRNAs, and 247 sense-overlapping lncRNAs. Principal component analyses revealed that lncRNA and mRNA expression profiles can effectively differentiate HCC with MVI from the controls Fig. 1A and B). After the screening of differentially expressed lncRNAs and mRNAs by the filter criteria ($P < 0.05$ and $|\log_{2}\text{fold change}| > 1$), 2005 and 8533 aberrantly expressed lncRNA and mRNA transcripts were identified, respectively. The volcano plots demonstrated significantly distinct expression signatures of these lncRNAs and mRNAs in the HCC with MVI compared with the control samples Fig. 1C and D). The hierarchical clustering results (Fig. 1E and F) revealed that the expression patterns of lncRNAs and mRNAs can largely distinguish HCC with MVI and ANLT groups. Circos plots representing the chromosome distribution of

A



B



C

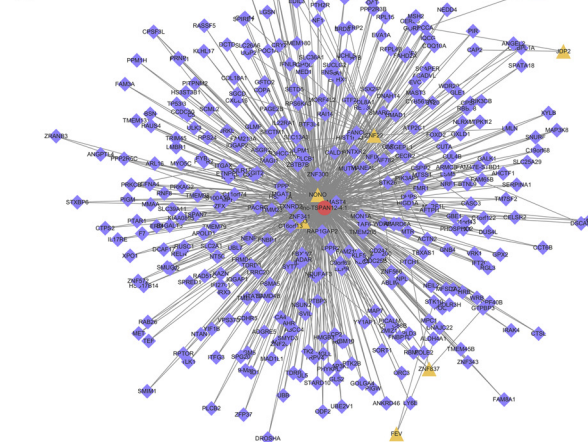


Fig. 5. Co-expression relationships between lncRNAs and mRNAs. (A) Differentially expressed lncRNA-mRNA co-expression network. Red and green node represented differentially expressed lncRNAs and mRNAs, respectively. (B) The correlation analysis of *lnc-TSPAN12*-predicted co-expression genes. Red and green indicated up- and down-regulation, respectively. (C) The regulatory network of transcription factors significantly correlated with *lnc-TSPAN12*. Red, yellow and purple node represented *lnc-TSPAN12*, transcription factors, and genes, respectively.

differentially expressed lncRNAs and mRNAs are illustrated in Fig. 2. The top 20 significantly dysregulated lncRNAs and mRNAs are listed in Supplementary Tables S3 and S4, respectively.

3.2. GO and KEGG analyses

The screened differentially expressed genes were further analyzed using bioinformatic tools. The GO functional annotations of differentially expressed mRNAs suggested that the most enriched biological processes were the epithelial cell apoptotic process involved in palatal shelf morphogenesis, the negative regulation of centriole–centriole cohesion, and the negative regulation of the cellular response to heat (Fig. 3A). KEGG pathway analysis showed that significantly differentially expressed genes might have influenced several cancer-related pathways, including cell cycle, DNA replication, mismatch repair, p53 signaling pathway, PI3K/Akt signaling pathway, ECM-receptor interaction, AMPK signaling pathway, and focal adhesion (Fig. 3B).

3.3. Real-time PCR validation of lncRNA expression

To validate the aberrant expression of lncRNAs found by RNA-seq,

we randomly selected eight lncRNAs from the top 20 upregulated lncRNAs (Fig. 4A). We performed qRT-PCR to examine the levels of *lnc-C1orf96-1*, *ST8SIA6-AS1*, *lnc-POTE*, *lnc-SEPT7L*, *LINC00355*, *lnc-NUAK1*, *lnc-DSCR8*, and *lnc-TSPAN12* in another 10 pairs of HCC with MVI and ANLT. The expression trend of the eight lncRNAs was consistent with the RNA-seq results, except for the decreased expression of *lnc-SEPT7L* (Fig. 4B). Among these lncRNAs, the novel *lnc-TSPAN12* attracted our attention because of its unknown role in HCC progression. As shown in Fig. 4B, *lnc-TSPAN12* was one of the most significantly upregulated lncRNA in qRT-PCR validation. Bioinformatic analyses further indicated that *lnc-TSPAN12* might be involved in cell adhesion, chemotaxis, and chemokine signaling pathway, which are closely related to the invasion and metastasis of HCC (Fig. 4C and D). Therefore, to explore the functional roles of *lnc-TSPAN12* in HCC progression, we selected *lnc-TSPAN12* as a candidate lncRNA for further investigation. *Lnc-TSPAN12* resides at chromosome 7q31.31, with a full-length sequence of 1 577 bp (Fig. 4E). By analyzing the sequence of *lnc-TSPAN12* using CPAT website (<http://lilab.research.bcm.edu/cpat/index.php>), we determined that *lnc-TSPAN12* has no ability to encode proteins (Fig. 4F).

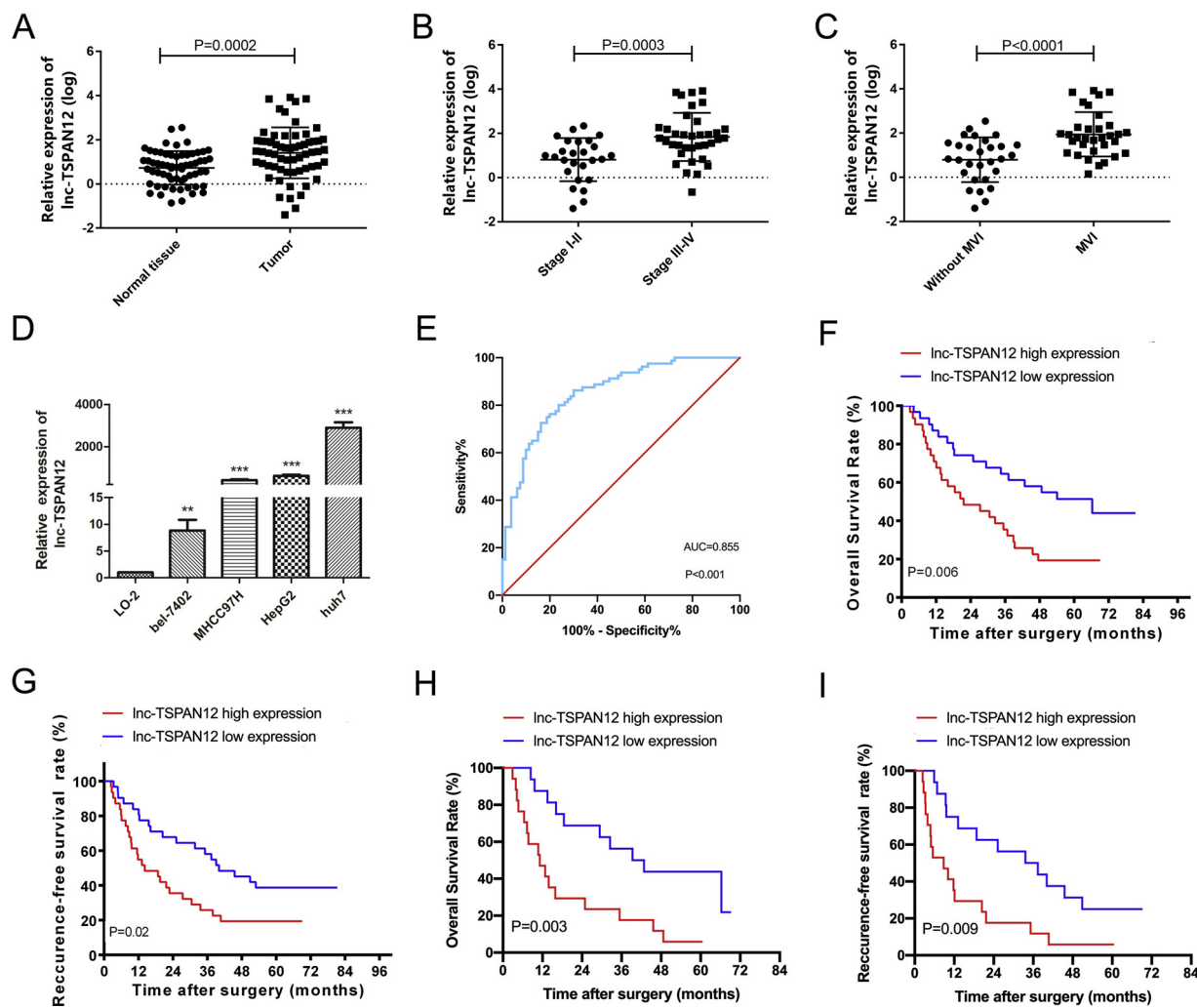


Fig. 6. *Lnc-TSPAN12* is significantly up-regulated in HCC and could serve as diagnostic and prognostic biomarker for HCC with MVI. (A) *Lnc-TSPAN12* expression was significantly overexpressed in HCC tissues compared with that in ANLT. (B) Expression levels of *Lnc-TSPAN12* was increased with advanced TNM stages. (C) *Lnc-TSPAN12* expression was obviously increased in HCC with MVI compared with HCC without MVI. (D) *Lnc-TSPAN12* expression was significantly increased in different HCC cell lines compared with normal human hepatic cell line. (E) ROC analysis of *Lnc-TSPAN12* expression in HCC with MVI and ANLT. (F, G) Kaplan-Meier analysis of OS and RFS between high and low expression levels of *Lnc-TSPAN12* in HCC patients. (H, I) Kaplan-Meier analysis of OS and RFS between high and low *Lnc-TSPAN12* expression levels in HCC with MVI patients. ** $P < 0.01$, *** $P < 0.001$.

3.4. Co-expression relationships between lncRNAs and mRNAs

To identify potential interactions between differentially expressed lncRNAs and mRNAs, we constructed the lncRNA-mRNA coexpression network according to an absolute value of the Pearson's correlation coefficient ≥ 0.80 and a P -value < 0.05 . Fig. 5A shows the lncRNA-mRNA co-expression network that consisted of the top 500 matched lncRNA-mRNA pairs representing 58 differentially expressed lncRNAs. To explore the internal mechanisms of *Lnc-TSPAN12* in HCC, we identified *Lnc-TSPAN12*-predicted co-expression genes through a correlation analysis (Fig. 5B). The transcription factors that might be strongly correlated with *Lnc-TSPAN12* were also predicted by the intersection between the set of co-expressed coding genes of lncRNA and the set of target genes of the transcription factors (Fig. 5C).

3.5. *Lnc-TSPAN12* is significantly upregulated in HCC and correlated with HCC progression

To determine the expression level and clinical significance of *Lnc-TSPAN12* in HCC, we performed qRT-PCR to detect its level in 62 matched pairs of randomly selected HCC tissues and their corresponding ANLT. Our results demonstrated that the *Lnc-TSPAN12*

expression was significantly overexpressed in 72.6 % (45/62) of HCC tissues compared with that in ANLT ($P = 0.002$, Fig. 6A). The expression level of *Lnc-TSPAN12* showed an increasing tendency with advanced TNM stages. As shown in Fig. 6B, the expression level of *Lnc-TSPAN12* in stage III/IV patients was significantly higher than that in stage I/II patients. Furthermore, the *Lnc-TSPAN12* expression was increased in HCC with MVI when compared with HCC without MVI (Fig. 6C, $P < 0.001$). Next, we evaluated the correlation between *Lnc-TSPAN12* expression and clinicopathologic features. Depending on the median expression level of the qRT-PCR results, all 62 patients were divided into high- and low-expression groups on the basis of the cut-off values, which were determined as the median level of *Lnc-TSPAN12* expression in HCC tissues. The overexpression of *Lnc-TSPAN12* in HCC tissues was strongly associated with large tumor size, macrovascular invasion, MVI, and advanced TNM stage ($P < 0.05$, Table 1).

Similarly, *Lnc-TSPAN12* was also significantly increased in different HCC cell lines compared with the normal human hepatic cell line LO2 ($P < 0.05$, Fig. 6D). These results suggest that upregulated *Lnc-TSPAN12* might play a critical role in HCC progression.

Table 2

Univariate and multivariate analysis of prognostic factors influencing OS of HCC.

Variables	n	Univariate analysis		Multivariate analysis	
		Survival (months)	P	HR (95 % CI)	P
Age (years)					
< 50	36	30.6	0.702		
≥ 50	26	37.2			
Gender					
Male	47	34.5	0.439		
Female	15	42.8			
AFP (ng/ml)					
< 20	18	30.6	0.912		
≥ 20	44	35.4			
Tumor size (cm)					
≤ 5	20	48.7	0.154		
> 5	42	29.4			
Lesion number					
Single	45	45.6	0.013	2.937(1.260–6.846)	0.013
Multiple	17	18.3			
Capsule formation					
No	37	30.6	0.137		
Yes	25	47.5			
Macrovascular invasion					
No	38	47.5	0.009	2.972(1.157–7.634)	0.024
Yes	24	16.1			
Microvascular invasion					
No	29	54.1	0.008	2.047(1.063–3.940)	0.032
Yes	33	18.5			
TNM staging					
I/II	26	54.1	0.007	1.293(0.469–3.568)	0.619
III/IV	36	20.4			
Edmonson-Steiner grade					
I-II	30	48.7	0.010	1.547(0.769–3.113)	0.221
III-V	32	18.3			
<i>lnc-TSPAN12</i> expression					
Low	31	54.1	0.006	2.924(1.460–5.855)	0.002
High	31	21.6			

HCC, hepatocellular carcinoma; OS, overall survival; AFP, alpha-fetoprotein.

3.6. *Lnc-TSPAN12* can serve as a potential diagnostic biomarker for HCC with MVI

To explore the diagnostic potential of *lnc-TSPAN12* in HCC with MVI, we performed a receiver operating characteristic (ROC) curve analysis in another cohort of 80 pairs of HCC with MVI and their corresponding ANLT. As shown in Fig. 6E, the *lnc-TSPAN12* expression was able to significantly discriminate HCC with MVI from ANLT with an AUC of 0.855 (sensitivity: 76.3 %, specificity: 80.0 %, 95 % CI: 0.797–0.912), suggesting that *lnc-TSPAN12* could serve as a diagnostic biomarker in HCC with MVI.

3.7. *Lnc-TSPAN12* overexpression predicts poor prognosis in HCC, including HCC with MVI

Kaplan-Meier survival analysis revealed that the patients with HCC and high *lnc-TSPAN12* expression levels were significantly correlated with decreased OS and RFS rates ($P = 0.006$ and $P = 0.02$, respectively; Fig. 6F and G) compared with those with low *lnc-TSPAN12* expression levels. Multivariable Cox proportional hazard regression analysis revealed that the high *lnc-TSPAN12* expression level in HCC tissues was an independent predictor for decreased OS and RFS ($P = 0.002$ and $P = 0.006$, respectively; Tables 2 and 3). We also found that the high *lnc-TSPAN12* expression in HCC with MVI predicted a worse prognosis than the low *lnc-TSPAN12* expression (Fig. 6H and I).

Table 3

Univariate and multivariate analysis of prognostic factors influencing RFS of HCC.

Variables	n	Univariate analysis		Multivariate analysis	
		Survival (months)	p	HR (95 % CI)	p
Age (years)					
< 50	36	21.7	0.713		
≥ 50	26	31.7			
Gender					
Male	47	20.4	0.467		
Female	15	37.4			
AFP (ng/ml)					
< 20	18	22.8	0.848		
≥ 20	44	25.2			
Tumor size (cm)					
≤ 5	20	35.2	0.112		
> 5	42	20.4			
Lesion number					
Single	45	35.2	0.005	2.285(0.985–5.300)	0.054
Multiple	17	14.2			
Capsule formation					
No	37	21.7	0.154		
Yes	25	37.9			
Macrovascular invasion					
No	38	35.2	0.004	2.115(0.889–5.030)	0.090
Yes	24	10.1			
Microvascular invasion					
No	29	39.1	0.005	2.036(1.072–3.869)	0.030
Yes	33	13.2			
TNM staging					
I/II	26	54.1	< 0.001	1.223(0.463–3.228)	0.685
III/IV	36	13.2			
Edmonson-Steiner grade					
I-II	30	40.7	< 0.001	2.047(1.017–4.121)	0.045
III-V	32	14.2			
<i>lnc-TSPAN12</i> expression					
Low	31	40.1	0.020	2.512(1.301–4.851)	0.006
High	31	14.2			

HCC, hepatocellular carcinoma; RFS, recurrence-free survival; AFP, alpha-fetoprotein.

3.8. *Lnc-TSPAN12* knockdown suppresses the migration and invasion of HCC cells in vitro

To further investigate the biological functions of *lnc-TSPAN12* in HCC progression, we transfected the Huh7 cell, which had the highest *lnc-TSPAN12* expression level with three specific shRNA lentiviruses targeting *lnc-TSPAN12*. As detected by qRT-PCR, *lnc-TSPAN12* was effectively knocked down in the Huh7 cell ($P < 0.001$, Fig. 7A). We selected Lv-*lnc-TSPAN12*-KD#1 for the subsequent experiments due to its highest knockdown efficiency. Cell proliferation was measured via the CCK-8 assay, and *lnc-TSPAN12* knockdown had no significant effect on cell proliferation in the Huh7 cell (Fig. 7B). However, *lnc-TSPAN12* knockdown remarkably suppressed Huh7 cell migration and invasion (Fig. 7C). These findings indicate that *lnc-TSPAN12* could promote the progression of HCC cells in vitro, which is consistent with the clinical results.

4. Discussion

Given the importance of determining the prognosis of patients with HCC, several preoperative scoring systems and imaging biomarkers have been established to predict the MVI and prognosis of patients with HCC [18–21]. However, the underlying molecular mechanism has not been fully clarified. Dysregulation of lncRNAs plays a crucial role in the

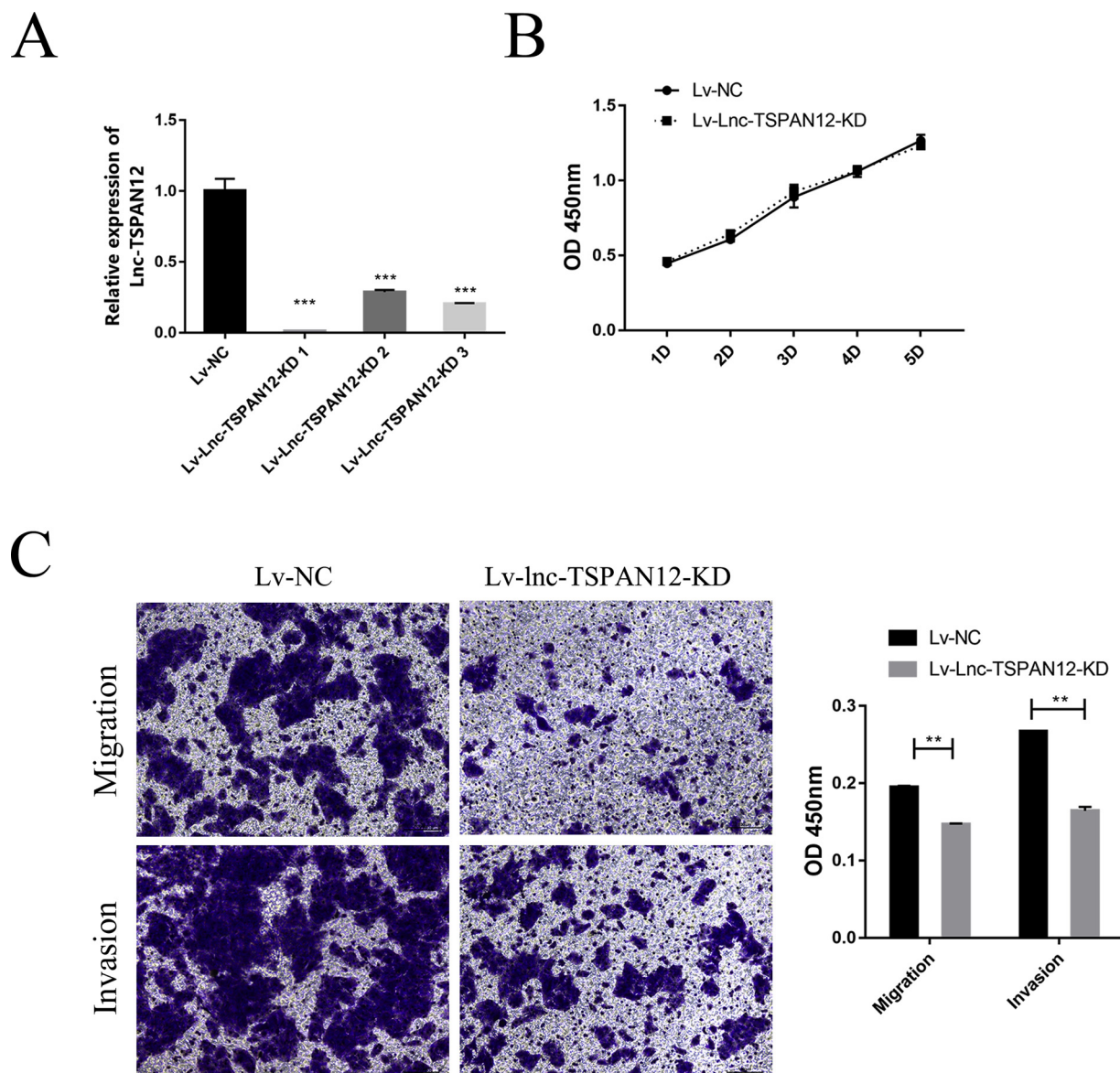


Fig. 7. *Lnc-TSPAN12* knockdown suppresses migration and invasion of HCC cell in vitro. (A) *Lnc-TSPAN12* was significantly knocked down in *lnc-TSPAN12* RNAi lentivirus infected Huh7 cell. (B) CCK-8 assay of Huh7 cell transfected with Lv-NC (empty lentivirus) or Lv-*Lnc-TSPAN12*-KD#1. (C) Transwell migration and invasion assays of Huh7 cell transfected with Lv-NC (empty lentivirus) or Lv-*Lnc-TSPAN12*-KD#1. **P < 0.01, ***P < 0.001.

carcinogenesis and progression of HCC [11,12,14]. However, the expression patterns and functions of lncRNAs in HCC with MVI are still largely unknown. In the present study, we established an integrative lncRNA and mRNA expression profile of HCC with MVI by using high-throughput RNA-seq and identified a collection of novel HCC-implied lncRNAs. Our data suggested that numerous lncRNAs were significantly differentially expressed between HCC with MVI and ANLT, thus providing evidence on the importance of lncRNAs in HCC with MVI. In addition, we found that several previously reported HCC-related lncRNAs, such as LINC01296 [22] and LINC01287 [23], exhibit an aberrant expression pattern. To validate the reliability of the RNA-seq results, we randomly selected eight lncRNAs from the top 20 up-regulated lncRNAs for qRT-PCR detection. The results were highly consistent with the RNA-seq data.

Bioinformatic analyses were performed to explore the potential biological functions of differentially expressed lncRNAs and mRNAs in HCC with MVI. The KEGG analysis results revealed that significantly differentially expressed mRNAs were involved in several well-known cancer-related pathways, such as cell cycle, ECM-receptor interaction,

focal adhesion, and p53, PI3K-Akt, and AMPK signaling pathways. Co-expression networks have been established to identify important mRNAs associated with cancer and predict the functions of the lncRNAs involved with them. In the present study, the lncRNA-mRNA co-expression network was constructed in HCC with MVI, and the result indicated that several hub lncRNAs and mRNAs might be involved in it. However, the exact function and mechanism of the lncRNA-mRNA co-expression network remains to be further investigated.

An increasing number of studies have demonstrated that lncRNAs could serve as ideal biomarkers and therapeutic targets for HCC [24–26]. In the present study, *Lnc-TSPAN12*, which was the most significantly upregulated lncRNA in the qRT-PCR validation, acted as a tumor promoter in HCC with MVI. Our qRT-PCR results indicated that *Lnc-TSPAN12* was significantly upregulated in HCC tissues, including HCC with MVI, and cell lines. After stratification by TNM stage, *Lnc-TSPAN12* level showed an increased tendency of the advanced TNM stage. Moreover, we found that *Lnc-TSPAN12* overexpression was significantly associated with large tumor size, macrovascular invasion, MVI, and advanced TNM stage. *Lnc-TSPAN12* overexpression also

predicted poor prognosis in patients with HCC, including HCC with MVI, and was an independent prognostic factor for OS and RFS in HCC. Function bioinformatic analysis based on the co-expression *lnc-TSPAN12*-mRNA network showed that *lnc-TSPAN12* had a correlation with tumor growth, invasion, epithelial-mesenchymal transition, and metastasis. Although the knockdown of *lnc-TSPAN12* had no obvious impact on cell proliferation in HCC cell, it remarkably suppressed cell migration and invasion ability in vitro. These data strongly suggest that *lnc-TSPAN12* may function as an oncogene in HCC progression and could serve as an effective prognostic predictor and a promising therapeutic target for HCC with MVI. However, the exact regulatory mechanism of *lnc-TSPAN12* in HCC with MVI is still unclear. Further functional and mechanistic studies on *lnc-TSPAN12* should be conducted.

ROC curve analysis was performed to determine the diagnostic value of *lnc-TSPAN12* in HCC with MVI. Our data indicated that *lnc-TSPAN12* could effectively distinguish HCC with MVI from ANLT with high sensitivity and specificity. Therefore, *lnc-TSPAN12* can be regarded as a potential diagnostic biomarker in HCC with MVI. Future studies with large sample sizes are necessary to evaluate the practical value of *lnc-TSPAN12* and verify it in the plasma of patients with HCC with MVI. Exosomal lncRNAs are also promising biomarkers for cancer diagnosis and prognosis [27–30]. Notably, our *lnc-TSPAN12* GO functional annotations revealed that extracellular exosome was one of the most significantly enriched GO terms in the cellular component. Hence, whether *lnc-TSPAN12* is present in tumor-derived exosomes and whether exosomal *lnc-TSPAN12* is also related to HCC progression need to be explored.

In conclusion, our study revealed the differential expression profiles of lncRNA and mRNA in HCC with MVI and their corresponding ANLT by using high-throughput RNA-seq. Bioinformatic analyses indicated that these dysregulated lncRNAs and mRNAs may play crucial roles in HCC tumorigenesis and development. *Lnc-TSPAN12* was highly expressed in HCC, including HCC with MVI, and associated with unfavorable clinicopathological features and poor prognosis. Our findings suggest that *lnc-TSPAN12* may contribute to HCC progression, thereby providing a novel diagnostic/prognostic biomarker and a potential therapeutic target for HCC with MVI.

Author contribution

Nansheng Cheng and Jiong Lu conceived and designed the study. Jiong Lu and Bei Li performed the experiments. Jiong Lu, Bei Li, and Xianze Xiong collected and analyzed the data. Jiong Lu and Nansheng Cheng drafted the manuscript.

Funding

This work was supported by the National Natural Science Foundation of China (Grant No. 81900516); the Science and Technology Supportive Plan of Sichuan Province (Grant No. 2019YFS0041, 2018SZ0170 and 2018SZ0195).

Declaration of Competing Interest

The authors declare no conflict of interest.

Acknowledgment

We thank Shanghai R&S Biotechnology Co., Ltd for technical assistance.

Appendix A. Supplementary data

Supplementary material related to this article can be found, in the

online version, at doi:<https://doi.org/10.1016/j.bioph.2020.110111>.

References

- [1] F. Bray, J. Ferlay, I. Soerjomataram, R.L. Siegel, L.A. Torre, A. Jemal, Global cancer statistics 2018: GLOBOCAN estimates of incidence and mortality worldwide for 36 cancers in 185 countries, CA Cancer J. Clin. 68 (6) (2018) 394–424, <https://doi.org/10.3322/caac.21492>.
- [2] A. Forner, J.M. Llovet, J. Bruix, Hepatocellular carcinoma, Lancet 379 (9822) (2012) 1245–1255, [https://doi.org/10.1016/S0140-6736\(11\)61347-0](https://doi.org/10.1016/S0140-6736(11)61347-0).
- [3] M. Maluccio, A. Covey, Recent progress in understanding, diagnosing, and treating hepatocellular carcinoma, CA Cancer J. Clin. 62 (6) (2012) 394–399, <https://doi.org/10.3322/caac.21161>.
- [4] K.C. Lim, P.K. Chow, J.C. Allen, G.S. Chia, M. Lim, P.C. Cheow, et al., Microvascular invasion is a better predictor of tumor recurrence and overall survival following surgical resection for hepatocellular carcinoma compared to the Milan criteria, Ann. Surg. 254 (1) (2011) 108–113, <https://doi.org/10.1097/SLA.0b013e31821ad884>.
- [5] S. Lee, T.W. Kang, K.D. Song, M.W. Lee, H. Rhim, H.K. Lim, et al., Effect of microvascular invasion risk on early recurrence of hepatocellular carcinoma after surgery and radiofrequency ablation, Ann. Surg. (2019), <https://doi.org/10.1097/SLA.0000000000003268> in press.
- [6] D.J. Erstad, K.K. Tanabe, Prognostic and therapeutic implications of microvascular invasion in hepatocellular carcinoma, Ann. Surg. Oncol. 26 (5) (2019) 1474–1493, <https://doi.org/10.1245/s10434-019-07227-9>.
- [7] Kopp F, J.T. Mendell, Functional classification and experimental dissection of long noncoding RNAs, Cell 172 (3) (2018) 393–407, <https://doi.org/10.1016/j.cell.2018.01.011>.
- [8] B. Uszczynska-Ratajczak, J. Lagarde, A. Frankish, R. Guigo, R. Johnson, Towards a complete map of the human long non-coding RNA transcriptome, Nat. Rev. Genet. 19 (9) (2018) 535–548, <https://doi.org/10.1038/s41576-018-0017-y>.
- [9] M.K. Iyer, Y.S. Niknafs, R. Malik, U. Singhal, A. Sahu, Y. Hosono, et al., The landscape of long noncoding RNAs in the human transcriptome, Nat. Genet. 47 (3) (2015) 199–208, <https://doi.org/10.1038/ng.3192>.
- [10] A.M. Schmitt, H.Y. Chang, Long noncoding RNAs in cancer pathways, Cancer Cell 29 (4) (2016) 452–463, <https://doi.org/10.1016/j.ccr.2016.03.010>.
- [11] Y.L. Wang, J.Y. Liu, J.E. Yang, X.M. Yu, Z.L. Chen, Y.J. Chen, et al., Lnc-UCID promotes G1/S transition and hepatoma growth by preventing DHX9-Mediated CDK6 down-regulation, Hepatology 70 (1) (2019) 259–275, <https://doi.org/10.1002/hep.30613>.
- [12] Y.H. Lin, M.H. Wu, Y.H. Huang, C.T. Yeh, M.L. Cheng, H.C. Chi, et al., Taurine up-regulated gene 1 functions as a master regulator to coordinate glycolysis and metastasis in hepatocellular carcinoma, Hepatology 67 (1) (2018) 188–203, <https://doi.org/10.1002/hep.29462>.
- [13] S.X. Yuan, F. Yang, Y. Yang, Q.F. Tao, J. Zhang, G. Huang, et al., Long noncoding RNA associated with microvascular invasion in hepatocellular carcinoma promotes angiogenesis and serves as a predictor for hepatocellular carcinoma patients' poor recurrence-free survival after hepatectomy, Hepatology 56 (6) (2012) 2231–2241, <https://doi.org/10.1002/hep.25895>.
- [14] J.L. Huang, S.W. Cao, Q.S. Ou, B. Yang, S.H. Zheng, J. Tang, et al., The long non-coding RNA PTTG3P promotes cell growth and metastasis via up-regulating PTTG1 and activating PI3K/AKT signaling in hepatocellular carcinoma, Mol. Cancer 17 (1) (2018) 93, <https://doi.org/10.1186/s12943-018-0841-x>.
- [15] J. Brown, M. Purrung, L. McCue, FQC Dashboard: integrates FastQC results into a web-based, interactive, and extensible FASTQ quality control tool, Bioinformatics 33 (19) (2017) 3137–3139, <https://doi.org/10.1093/bioinformatics/btx373>.
- [16] A.M. Bolger, M. Lohse, B. Usadel, Trimmomatic: a flexible trimmer for Illumina sequence data, Bioinformatics 30 (15) (2014) 2114–2120, <https://doi.org/10.1093/bioinformatics/btu170>.
- [17] D. Kim, B. Langmead, S.L. Salzberg, HISAT: a fast spliced aligner with low memory requirements, Nat. Methods 12 (4) (2015) 357–360, <https://doi.org/10.1038/nmeth.3317>.
- [18] X.P. Zhang, K. Wang, X.B. Wei, L.Q. Li, H.C. Sun, T.F. Wen, et al., An eastern hepatobiliary surgery hospital microvascular invasion scoring system in predicting prognosis of patients with hepatocellular carcinoma and microvascular invasion after R0 liver resection: a large-scale, multicenter study, Oncologist 24 (12) (2019) e1476–e1488, <https://doi.org/10.1634/theoncologist.2018-0868>.
- [19] S. Lee, S.H. Kim, J.E. Lee, D.H. Sinn, C.K. Park, Preoperative gadoxetic acid-enhanced MRI for predicting microvascular invasion in patients with single hepatocellular carcinoma, J. Hepatol. 67 (3) (2017) 526–534, <https://doi.org/10.1016/j.jhep.2017.04.024>.
- [20] X. Xu, H.L. Zhang, Q.P. Liu, S.W. Sun, J. Zhang, F.P. Zhu, et al., Radiomic analysis of contrast-enhanced CT predicts microvascular invasion and outcome in hepatocellular carcinoma, J. Hepatol. 70 (6) (2019) 1133–1144, <https://doi.org/10.1016/j.jhep.2019.02.023>.
- [21] T. Ryu, Y. Takami, Y. Wada, M. Tateishi, T. Hara, M. Yoshitomi, et al., A clinical scoring system for predicting microvascular invasion in patients with hepatocellular carcinoma within the Milan criteria, J. Gastrointest. Surg. 23 (4) (2019) 779–787, <https://doi.org/10.1007/s11605-019-04134-y>.
- [22] Y.F. Wan, M.L. Li, P. Huang, LINC01296 promotes proliferation, migration, and invasion of HCC cells by targeting miR-122-5P and modulating EMT activity, Onco. Ther. 12 (2019) 2193–2203, <https://doi.org/10.2147/OTT.S197338>.
- [23] Y.C. Mo, L.G. He, Z.R. Lai, Z.H. Wan, Q.S. Chen, S.B. Pan, et al., LINC01287/miR-298/STAT3 feedback loop regulates growth and the epithelial-to-mesenchymal transition phenotype in hepatocellular carcinoma cells, J. Exp. Clin. Cancer Res. 37 (1) (2018) 149, <https://doi.org/10.1186/s13046-018-0831-2>.

- [24] Y. Wang, W.J. Li, X.Y. Chen, Y. Li, P.H. Wen, F. Xu, MIR210HG predicts poor prognosis and functions as an oncogenic lncRNA in hepatocellular carcinoma, *Biomed. Pharmacother.* 111 (2019) 1297–1301, <https://doi.org/10.1016/j.biopha.2018.12.134>.
- [25] M. Klingenberg, A. Matsuda, S. Diederichs, T. Patel, Non-coding RNA in hepatocellular carcinoma: mechanisms, biomarkers and therapeutic targets, *J. Hepatol.* 67 (3) (2017) 603–618, <https://doi.org/10.1016/j.jhep.2017.04.009>.
- [26] J.C. Wang, J. Pu, T.W. Yao, X.J. Lu, Y.B. Deng, Four long noncoding RNAs as potential prognostic biomarkers for hepatocellular carcinoma, *J. Cell. Physiol.* 234 (6) (2019) 8709–8716, <https://doi.org/10.1002/jcp.27530>.
- [27] L.J. Huang, Y. Wang, J. Chen, Y. Wang, Y.B. Zhao, Y.L. Wang, et al., Long non-coding RNA PCAT1, a novel serum-based biomarker, enhances cell growth by sponging miR-326 in oesophageal squamous cell carcinoma, *Cell Death Dis.* 10 (7) (2019) 513, <https://doi.org/10.1038/s41419-019-1745-4>.
- [28] C.L. Li, Y.L. Lv, C.Y. Shao, C. Chen, T.L. Zhang, Y.Q. Wei, et al., Tumor-derived exosomal lncRNA GAS5 as a biomarker for early-stage non-small-cell lung cancer diagnosis, *J. Cell. Physiol.* 234 (11) (2019) 20721–20727, <https://doi.org/10.1002/jcp.28678>.
- [29] Y.R. Lee, G. Kim, W.Y. Tak, S.Y. Jang, Y.O. Kweon, J.G. Park, et al., Circulating exosomal noncoding RNAs as prognostic biomarkers in human hepatocellular carcinoma, *Int. J. Cancer* 144 (6) (2019) 1444–1452, <https://doi.org/10.1002/ijc.31931>.
- [30] L.Y. Lin, L. Yang, Q. Zeng, L. Wang, M.L. Chen, Z.H. Zhao, et al., Tumor-originated exosomal lncUEGCI as a circulating biomarker for early-stage gastric cancer, *Mol. Cancer* 17 (1) (2018) 84, <https://doi.org/10.1186/s12943-018-0834-9>.